

DYNAMIC LOADING ON TURBOFAN BLADES DUE TO BIRD-STRIKE

Sunil K. Sinha

GE Aviation, General Electric Company
Cincinnati, OH 45215, U.S.A.

Kevin E. Turner

GE Aviation, General Electric Company
Cincinnati, OH 45215, U.S.A.

Nitesh Jain

Bangalore Engineering Center, JFWTC
Bangalore-560066, Karnataka, India

ABSTRACT

In the present paper, a hydrodynamic bird material model made up of water and air mixture is developed, which produces good correlation with the measured strain-gage test data in a panel test. This parametric bird projectile model is used to generate the time-history of the transient dynamic loads on the turbofan engine blades for different size birds impacting at varying span locations of the fan blade. The problem is formulated in 3-D vector dynamics equations using a non-linear trajectory analysis approach. The analytical derivation captures the physics of the slicing process by considering the incoming bird in the shape of a cylindrical impactor as it comes into contact with the rotating fan blades modeled as a pre-twisted plate with a camber. The contact-impact dynamic loading on the airfoil produced during the bird-strike is determined by solving the coupled non-linear dynamical equations governing the movement of the bird-slice in time-domain using a sixth-order Runge-Kutta technique. The analytically predicted family of load time-history curves enables the blade designer to readily identify the critical impact location for peak dynamic loading condition during the bird-ingestion tests mandated for certification by the regulatory agencies.

1. INTRODUCTION

During the routine operating conditions of a commercial engine, there is a likelihood of encountering many different types of foreign object damage called FOD. Foreign object damage (FOD) in a turbofan engine component can be classified under two major categories: (a) soft-body impact and

(b) hard-body impact. The most prevalent example of engine soft-body damage in civil aviation is caused by the ingestion of a bird or flock of birds, which is commonly referred to as bird-strike. Due to noise concerns, the majority of airports being built today are positioned away from the heavily populated areas and closer to the natural habitat for wild birds. As a result, the number of recorded bird-strikes during commercial flights has increased dramatically in recent years. To combat this trend, the regulatory agencies continually review and revise their safety regulations regarding bird-strikes. The regulations generally state that turbofan blades must be able to withstand the impact from various size and quantities of birds without any disruption of the normal flight of the aircraft [1].

The dynamic forces being generated during a bird-strike on an engine blade are highly non-linear in nature, and until now no attempt has been made to determine these loads in any physics-based analytical model. Nearly all the analytical studies done to date have been carried out using finite-element techniques based upon time marching integration schemes with explicit formulation [2-19]. Soft-body impacts, as opposed to hard-body impacts, create additional challenges in any numerical technique due to the large distortion of the Lagrangian mesh used to simulate the soft-body. To overcome these challenges, several advanced numerical schemes, such as ALE (Arbitrary Lagrangian Eulerian) formulation [7], SPH (Single Particle Hydrodynamic) element, and adaptive meshing techniques, have been recommended by researchers in this field. These finite-element models are solved using commercial codes, such as LS-DYNA, and although they are highly accurate, the computation costs could be prohibitive due to extremely small time-step size required by the solver. In 1991, Teichman and Tadros [20] were among the first ones to

investigate the damage to turbo-engine fan blades due to bird-strike using analytical and experimental simulations. With the advancements in computational speed during the last 20 years, the three-dimensional bird-strike models impacting a fan blade [21] have become more detailed and sophisticated.

In a recent paper by Lavoie and his coworkers [22], they have provided a good review of all the different ways to represent the dynamic behavior of bird material in an analytical formulation. The precise determination of any impact-force has always been a challenge [23] and an earlier paper by Shivkumar and his colleagues [24] has been a significant contribution in that direction. Sinha and Zentner [25] used the Kirchoff-von Karman elastic plate bending equation to determine the impact-load and the stresses caused by a moving spherical projectile with a Hertzian contact formulation. Doyle [26] made an experimental determination of contact-impact forces on an orthotropic plate for a similar configuration. Hemni and his coworkers [27] presented the results of an analytical prediction of foreign object (FOD) impact force on a composite fan blade.

In any impact event, two objects are involved such that one object moving with higher relative velocity, called the projectile, comes into contact with another object, dubbed the target. Depending upon the orientation of the relative velocity vector with respect to the contact surface of the target, an impact event can be classified either as a 'normal impact' or an 'oblique impact'. Thus in a typical bird-strike scenario on a turbofan rotor, it is invariably an 'oblique impact' event with the bird acting as the projectile or impactor, and the fan blade being the target, which also acts as a slicer. In this process an incoming bird gets cut into multiple slices by the rotating blades, which dynamically load the fan blades as each individual bird-slice travels from the leading edge of the fan blade towards its trailing edge. Theoretically, the 'oblique impact' generates both normal and tangential components of the dynamic contact loads, however, because of the very short duration of the bird-strike event the normal forces due to inertia of the target are an order of magnitude higher than the corresponding tangential forces, which are resisted by the dynamic coefficient of friction at the blade pressure surface. In the high-velocity bird-strike simulations, it is a common practice to neglect the effect of friction at the contact surface, which has been found to be adequate through many numerical simulations and verifying with the test measurements of predicted peak strains both for near and far-field responses of the blade. The time duration of a typical contact-impact bird-loading on a fan blade may last anywhere from a fraction of millisecond to a few milliseconds. The peak magnitude of these dynamic loads can be of the order of 10^5 Newtons. However, the precise time-history of the transient dynamic loads have never been determined accurately due to its very short duration and highly non-linear nature of the bird-strike event.

This paper summarizes the first attempt made to determine the dynamic load-history on a fan blade in a semi-closed form by numerically solving the highly non-linear partial differential equations. The solution of partial differential equation helps in understanding the complex dynamics of a bird-strike on a twisted curved plate and also to carry out parametric studies, which can be difficult to complete using a finite-element based approach. In the present work, the bird has been modeled as a fluid with a mixture of water and air, which comes in contact with the airfoil blade that is modeled as an elastic material rotating in a centrifugal force field. The transient dynamic contact load being applied by the bird material on the pressure (concave) surface of the fan blade is treated as a travelling load vector acting in the direction normal to the surface. Here, it should be noted that due to relatively very short duration of bird-loading time being in the range of 1-2 m-seconds, the effect of dynamic coefficient of sliding friction is very-very minimal. As such in any typical bird-strike type impact simulation, the tangential component of the relative velocity is usually neglected. The instantaneous location of this external load vector with respect to the blade coordinates is determined by the nonlinear trajectory analysis of a moving mass on a curved and twisted surface rotating in space about the engine axis. In this paper we also discuss as to how these impulsive loads generated during the bird-strike can be used to develop a forcing function for determining the dynamic response of any generic pre-twisted fan blade in an aero-engine.

In this study, the bird is modeled in the shape of a circular cylinder made up of 10% air and 90% water. The current bird modeling approach has been verified by simulating, in LS-DYNA, the impact event of a controlled panel impact test. It is demonstrated that the substitute bird model used in generating the dynamic loads on the fan blade, presented in this paper, can replicate the test data very well.

2. EFFECT OF BIRD-STRIKE ON A TURBOFAN BLADED-ROTOR

Since the pioneering work of Wilbeck and Rand [28] on bird modeling, it has been established [29] that, in a soft-body impact (especially on a rotating structure such as fan and compressor blades), the slicing action of the ingested soft-object during the leading edge-impact generates maximum dynamic loads on the rotating airfoils. When a soft-body comes in contact with a rotating blade, there is a clear distinction in its dynamic response between the slicing and non-slicing impacts. It should be noted that majority of the high-velocity impact tests under controlled conditions have invariably been normal impact tests where the impactor hits the target, usually made up of a flat plate at 90-degrees to the in-plane surface. In interpreting the results of such commonly used plate impact tests, there has been an inherent assumption that a direct normal impact of a

target by a moving projectile should be the most damaging, which is not necessarily true in all soft-body impacts. In bird-strike and ice-impact situations, usually the slicing action of the rotor produces largest dynamic loads and the actual slice size becomes a critical parameter in predicting the amount of damage to a rotating engine component. A non-slicing impact in the middle of the blade surface is not the most conservative loading condition for the design of bird-strike tolerant fan blades. Thus, precise simulation of the slicing process is an important aspect of bird-strike analysis and is a prerequisite for accurate prediction of peak transient dynamic loads to which the fan blade will be subjected.

The level of blade damage due to bird-strike depends upon several impact-related scenarios, such as: the size of the bird, the quantity of birds, the radial location of impact, engine running speed, aircraft speed and slicing versus non-slicing impact. Depending upon the elastic flexibility of the blade, it may not be permanently damaged during the bird-strike but it will experience large deformation of the blade leading edge that may fully recover due to the nature of the elastic response in a centrifugal force field. This large transient deformation blocks the airflow-passage, which may cause momentarily thrust loss. In metal airfoils, due to ductility of the material, bird-impact may lead to a permanent plastic bulge at the leading edge of the blade (see Fig. 1) in the vicinity of initial contact that will block the air-flow without any possibility of recovery.



FIG. 1: A typical plastically deformed bulge in the leading edge of a metal turbfan blade after slicing action during bird-strike

On the other hand, in carbon-epoxy composite fan blades these damages can range from small surface indentation to delamination of the plies, fiber failure, matrix rupture or unbonding of the metal cladding. The damage in composite fan blades during the slicing action can be reduced by a metal cladding of the leading edge [8]. In addition, based upon the bird-size and the inlet area of the engine a bird can impact multiple blades in one sector of the bladed-rotor, which would create unacceptable levels of rotor imbalance. Thus, a bird-strike may not only result into sudden thrust loss, it could also apply significant torque and imbalance loads on the fan-shaft, which need to be considered during the design phase of these components.

2.1. Slicing action of a bird

Although a real life bird-strike can involve birds of many different species, shapes, sizes and orientations, for aerospace analysis purposes, considerable amount of research work has been done on developing a mathematical bird model [2-21], which is amenable to a classical impact analysis formulation comprising of an impactor and a target. The groundbreaking work of Wilbeck and Rand [28] showed that it was possible to model the bird as a cylinder made up of a mixture of water and air. Through a series of actual tests, he had demonstrated that such an impactor will generate a dynamic load time-history on fan blades that is representative of a real bird. As a result, in the current analysis, we will consider the incoming bird as made up of a mixture of water and air in the form of a circular cylinder with its length-to-diameter ratio of $(B_L/B_D) = 2.0$. In the turbfan design analysis, it is a standard practice to position the incoming bird in such a way that the bird-cylindrical axis is oriented along the engine axis.

In order to determine the magnitude of the transient dynamic contact-impact loads generated by the moving bird mass, it is important to establish certain mathematical parameters that capture the mechanics of the slicing action. The slice size is a function of various parameters such as: the number of blades on the fan rotor, rotational speed, and aircraft speed. For the purpose of analytical formulation (see Fig. 2), we consider a case where the bird of diameter B_D comes into contact with the airfoil blade at a span height 's' on a rotating bladed-rotor with N_b number of blades on it. The bird cylinder of length B_L moving with an axial velocity of V_a gets sliced into several pieces with the axial length of each slice given by

$$B_s = \frac{60V_a}{(\text{RPM})N_b} \quad (1)$$

[where, RPM = rotational speed of the fan rotor = $\frac{60\Omega}{2\pi}$].

From the geometrical profile of the blade, the 'stagger angle $\phi(s)$ ' at the impact location due to pre-twist in the airfoil is expressed as,

$$\phi(s) = \phi_0 + \phi' s \quad (2)$$

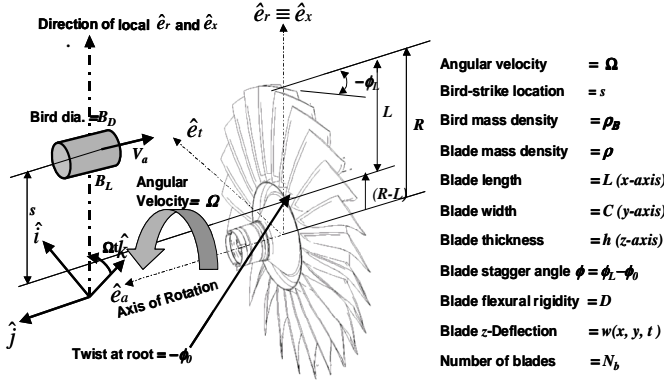


FIG. 2: Bird cylinder coming in contact with rotating turbofan blades and local coordinate system

Referring to Fig. 2 we start with rectangular cartesian coordinate system $(\hat{i}, \hat{j}, \hat{k})$ fixed in space with \hat{j} -direction coinciding with the engine axis. We also introduce two additional rotating curvilinear coordinate systems viz., $(\hat{e}_t, \hat{e}_a, \hat{e}_r)$ attached to the center of the fan shaft and the other $(\hat{e}_x, \hat{e}_y, \hat{e}_z)$ to the clamped-end of the cantilevered fan blade. Using the velocity triangle formed by the tangential velocity of the rotating blade V_t and the axial velocity of the aircraft V_a , the angle of the slice $\beta = \tan^{-1}(V_a/V_t)$ can easily be calculated from Fig. 3. Here the magnitude of tangential velocity V_t at the impact location of the blade leading edge is given by,

$$V_t = \Omega(R - L + s) = \frac{2\pi(\text{RPM})}{60}(R - L + s). \quad (3)$$

For majority of bird-strike scenarios, typical magnitude of V_t is usually much larger than V_a , which is usually in the range of only 100 m/s.

In Fig. 3 two different cut-slice shapes called 'Ideal slice' and 'Actual slice' are shown which are caused by the difference in the 'rigid blade' versus 'deformable blade' formulations. The 'Ideal slice' in the shape of a parallelogram can be formed, if the blade would have been 'perfectly rigid'. However as a result of deformable blade behavior, a transient

dynamic bulge is formed in the vicinity of the initial contact with the blade leading edge as the slicing process continues for a finite time-duration called ' t_{slicing} '.

Let us assume that for a typical bird-strike analysis we are considering a bird of mass B_M with its diameter being B_D and the length of the cylinder as B_L , then using ρ_B as the density of the bird material, we can write,

$$\text{bird mass } B_M = \rho_B \left[(\pi/4) B_D^2 B_L \right]. \quad (4)$$

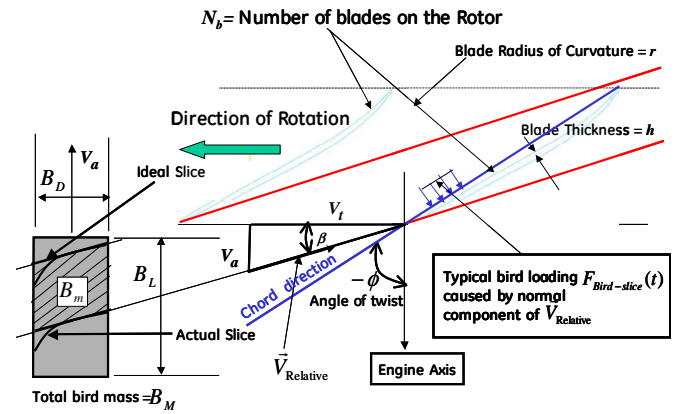


FIG. 3: Effect of relative velocity vector during slicing action of the fan blade

Then using $B_L/B_D = 2$, we can describe the bird cylindrical shape parameters as diameter and length as,

$$B_D = \left[\frac{2B_M}{\pi\rho_B} \right]^{1/3} \quad \text{and} \quad B_L = 2 \left[\frac{2B_M}{\pi\rho_B} \right]^{1/3}. \quad (5)$$

It should be noted that a large-size bird will have a longer cylindrical length B_L , which may result into multiple blades being fully or partially hit in one sector of the fan-rotor by a single bird. In that situation, one needs to determine number of fan blades coming in contact with the bird as:

Number of blades coming in contact with the bird

$$= \frac{B_L + C \cos(\phi_0 + \phi' s)}{V_a} \left[\frac{(\text{RPM}) N_b}{60} \right] \quad (6)$$

However in a typical bird-strike analysis for turbofan design, the interest is usually only in the blades which take the brunt of full-size slice as they might experience maximum damage. For

this reason, the number of blades being damaged or impacted is approximated as N_B which is given by,

$$N_B = \frac{B_L}{B_S} = \frac{B_L}{V_a} \left[\frac{(\text{RPM})N_b}{60} \right] \quad (7)$$

Also, from Eq. (1) we have,

$$\text{Bird slice mass } B_m = \rho_B \left[(\pi/4)B_D^2 \frac{60V_a}{(\text{RPM})N_b} \right] \quad (8)$$

The bird-slice or the point mass ' B_m ' experiences a complex combination of forces such as Coriolis forces, centripetal forces, and turning forces. In order to keep this analysis amenable to solution, we have made several assumptions, where the results may slightly deviate from a real-life bird-strike problem:

(a) Real blade deforms and a bulge is created near the impact area, thus changing the curvature of blade locally in the vicinity of the bird, however, in the present analysis the curved surface is assumed to be rigid and as such radius of curvature ' r ' for a given span location ' s ' is constant.

(b) Real bird has a finite size and spreads over a large area after the impact called bird's foot-print, but in the current analysis it is assumed to be concentrated at a point.

(c) Real bird starts coming into contact of the blade gradually until the entire bird has been squashed up against the pressure (concave) surface, however, in the current analysis it is assumed that the entire mass of the bird-slice loads the concave surface instantaneously.

2.2. Transient dynamic loads applied by the bird slice

The transient dynamic loads on the blade during bird-strike can be divided in two distinct phases: (a) slicing impact load at the leading edge of the blade (b) bird-slice turning load during sliding from the leading edge to the trailing edge of the blade. The dynamic characteristics of these two loads are discussed in detail in the following two sub-sections.

2.2.1. Slicing-impact load at the leading edge of the blade

During the slicing event as the first phase of impact loading, the dynamic forces are due to the stagnation pressure generated by a stream of moving fluid when it is stopped suddenly by a rigid wall. For determining the slicing stagnation

pressure $p_{\text{stagnation}}$ being generated at the contact location of the concave surface of the blade, we compute the impact velocity of the bird-slice as the normal component called ' V_{impact} ' with respect to the blade, which yields

$$p_{\text{stagnation}} = \frac{1}{2} \rho_B (V_{\text{impact}})^2 \quad (9)$$

where, the usual value of the fluid density term ρ_B for the bird material is 0.9 g/cm³.

The transient magnitude of the slicing load, henceforth called ' F_{slicing} ', is determined by computing the contact area of the blade pressure surface, referred to as the "bird-foot-print-area" represented by B_a , which in the numerical scheme is updated as the slicing action progresses, i.e.

$$F_{\text{slicing}}(t) = B_a(t) p_{\text{stagnation}} \quad (10)$$

The total duration of slicing is computed by the bird cylinder diameter B_D and the tangential velocity V_t of the blade leading edge at the contact location, given by

$$t_{\text{slicing}} = \frac{B_D}{V_t} \quad (11)$$

It should be noted that due to the contribution from the bird's axial velocity V_a , the relative velocity vector of the bird with respect to the blade changes direction, which results into the shape of the slice being in the form of a parallelogram with an angle of inclination being β . Thus the largest bird-foot-print area on the blade pressure surface is generated when the bird-cylinder is fully sliced from one side of the bird-cylinder to the other side by the relative velocity vector, and is computed as,

$$\text{Max. } B_a = \frac{B_A}{\cos \beta} = \frac{(\pi/4)B_D^2}{\cos \beta} \quad (12)$$

It should be noted that the cross-sectional area of the bird cylinder B_A is constant for a given bird-size, however, B_a representing the "bird-foot-print-area" is a function of time as the bird-cylinder gets sliced. Although for mathematical simplification purposes, the shape of the ideal slice is determined along a straight line cut in the direction of the relative velocity vector, the actual slice takes place on a slightly curved path due to the local deformation in the shape of bulge of the blade leading edge during the slicing action itself. It can be seen from Fig. 3 that due to this additional time-dependent non-linearity of the slicing action, the effective slice-mass in a

test environment is somewhat bigger than the "ideal" slice-size calculated in this manner. Depending upon the span location of the bird-impact, the leading edge velocity in the circumferential direction of the blade V_t at the initial contact location would be typically in the range of 200 m/sec to 400 m/sec. The magnitudes of other relevant velocities in a typical bird-strike event on a turbofan rotor blade are in the following ranges.

(a) Normal component V_{impact} of relative velocity $\vec{V}_{\text{Relative}}$ is usually 200 m/sec.

(b) Axial velocity of incoming bird V_a with respect to the fan blade is usually 70 -120 m/sec.

(c) Peak out-of-plane velocity of the blade pressure surface due to local elastic deformation is $[\dot{w}]_{\text{max}} = 20 - 70$ m/sec.

2.2.2. Bird-slice turning load during sliding from the leading edge to the trailing edge of the blade

The bird-slice coordinate location 'c' changes as a function of time as it travels from the blade leading edge to the blade trailing edge. Thus, the loading time for the blade is computed by the time it takes the bird-slice to travel or sweep through the chord of the blade, which is approximated by:

$$t_{\text{travel}} = \frac{C \cos \phi}{V_a}. \quad (13)$$

As the bird mass slides on the concave surface of the rotating blade after being sliced and moves from the leading edge towards the trailing edge of the blade, it generates large Coriolis forces. These Coriolis forces, represented by the term F_{travel} , are acting in the direction normal to the pressure surface of the blade; the other complimentary component of which propels the bird-mass towards the higher radius trajectory. Thus, the total blade loading time t_{loading} is the sum of two distinct actions on the bird, which is the slicing and the sweep time, namely,

$$t_{\text{loading}} = t_{\text{slicing}} + t_{\text{travel}} = \frac{B_D}{V_t} + \frac{C \cos \phi}{V_a} \quad (14)$$

Thus, the total transient loading on the pressure surface of the impacted blade, henceforth called $F_{\text{Bird-slice}}$, during the bird-strike event is the vector sum of these two loads, which is written as,

$$F_{\text{Bird-slice}} = F_{\text{slicing}} + F_{\text{travel}} \quad (15)$$

In the following section of this paper, we will use a rigid-body non-linear trajectory analysis to determine the time-history of the load magnitude $F_{\text{Bird-slice}}$ and the corresponding instantaneous bird-slice location (s, c) to solve for transient

dynamic response of the rotating fan blade. In the twisted-plate equation of motion, described in section-5 of this paper, the normal load vector $F_{\text{Bird-slice}}$ is applied as an external forcing function on the rotating blade in the form of a moving load.

3. BIRD-SLICE TRAJECTORY AND CONTACT-IMPACT DYNAMIC LOAD ON THE BLADE

In this section, we will develop some kinematical relationships in order to determine the bird-slice trajectory as it slides and travels from the front to the rear of the curved and pre-twisted airfoil. Here the dynamics of a point mass representing a bird slice, travelling on a concave curved and twisted surface is analyzed. We will also determine the relative velocity vector that applies the contact-impact load F_{travel} on the concave surface of the blade in that process. With that objective in mind, suppose the aircraft is moving with velocity V_a , then the components of the bird velocity vector \vec{V}_a in the blade coordinate system $(\hat{e}_x, \hat{e}_y, \hat{e}_z)$ is written as (see Fig. 3),

$$\vec{V}_a = -V_a \cos \phi \hat{e}_y + V_a \sin \phi \hat{e}_z. \quad (16)$$

Thus the velocity of bird-impact with respect to the rotating blade coordinate system will be:

$$\begin{aligned} & V_a \cos \phi \hat{e}_y - V_a \sin \phi \hat{e}_z \\ & = V_a [\cos(\phi_0 + \phi' s) \hat{e}_y - \sin(\phi_0 + \phi' s) \hat{e}_z] \end{aligned} \quad (17)$$

Let us assume that the bird makes initial contact with the leading edge of the rotating fan blade at a coordinate location (s, c) such that the span-wise location $x = s$ and, $y = c = -r \sin \theta$. Thus, the instantaneous position vector of the bird-slice $\vec{r}(s, \theta)$ in the blade curvilinear coordinate system (see Fig. 4) can be written as,

$$\begin{aligned} & \vec{r}(s, \theta) \\ & = s \hat{e}_x - r \sin \theta \hat{e}_y + [-r(1 - \cos \theta) + w] \hat{e}_z \end{aligned} \quad (18)$$

where, $\theta = -\sin^{-1} \left[\frac{c}{r} \right]$.

In the above equation 'w' is the out-of-plane elastic deformation of the blade due to the contact-impact traveling load vector defined in Eq. (15). In general the magnitude of the elastic deformation of the blade, 'w', will be very small with respect to the other parameters 's' and 'c' and therefore will be

disregarded for trajectory determination. Under this assumption the instantaneous position vector $\vec{\mathbf{r}}(s, \theta)$ of the bird slice in terms of blade coordinates (see Fig. 3) can be simplified as,

$$\vec{\mathbf{r}}(s, \theta) = s\hat{\mathbf{e}}_x - r \sin \theta \hat{\mathbf{e}}_y - r(1 - \cos \theta)\hat{\mathbf{e}}_z \quad (19)$$

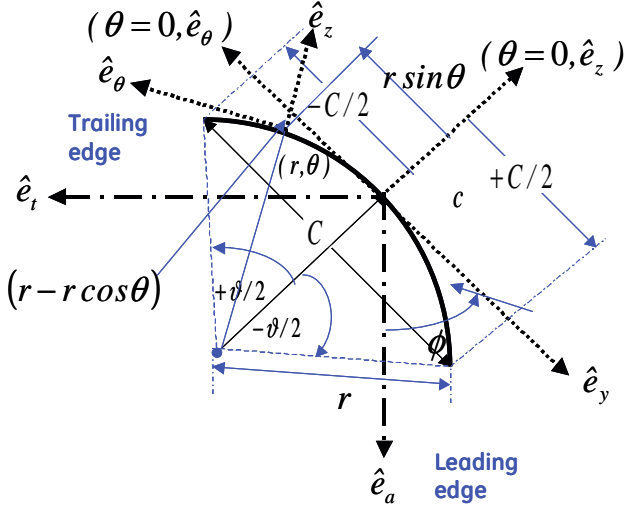


FIG. 4: A pre-twisted and curved airfoil surface as viewed from the blade tip-side

Also, the chord direction limits on the blade between the trailing edge (TE) and the leading edge (LE) varies between the limits of $-C/2 \leq c \leq +C/2$. In the current system, the leading edge is at $c = +C/2$ and the trailing edge of the blade is at $c = -C/2$. The corresponding limits in the local shell coordinates of θ -direction will be $\vartheta/2 \geq \theta \geq -\vartheta/2$, such that,

$$\vartheta = -2 \sin^{-1} \left[\frac{C_0 + C's}{2(r_0 + r's)} \right] \quad (20)$$

The curved surface, the cross-section of which is assumed to be in the form of an arc of a circle with radius ' r ' is considered to be spinning at a constant angular velocity ' Ω ' about the global Y -axis in the stationary frame of reference. The spinning surface representing the blade pressure surface is both curved and twisted in space such that both the radius of curvature ' r ' and the twist angle ' ϕ ' are functions of span height ' s ', which for $x = s$ can be written as,

$$r = r(x) = r_0 + r'x = r_0 + \frac{r_L - r_0}{L}x \quad (21)$$

and,

$$\phi = \phi(x) = \phi_0 + \phi'x = r_0 + \frac{\phi_L - \phi_0}{L}x \quad (22)$$

also,

$$x = s(t). \quad (23)$$

For the sake of convenience in mathematical derivations, we will use previously defined coordinate systems (see Fig. 2) attached to the running engine, henceforth called 'Tangential-Axial-Radial' system $(\hat{\mathbf{e}}_t, \hat{\mathbf{e}}_a, \hat{\mathbf{e}}_r)$ and the plate coordinates called 'Length-Width-Thickness' system $(\hat{\mathbf{e}}_x, \hat{\mathbf{e}}_y, \hat{\mathbf{e}}_z)$, respectively. Here, unit vectors $(\hat{\mathbf{e}}_t, \hat{\mathbf{e}}_a, \hat{\mathbf{e}}_r)$ are in the cylindrical coordinate system and as such are only functions of angular velocity Ω , whereas $\hat{\mathbf{e}}_z$ is normal to the mid-surface pointing away from the center of curvature, $\hat{\mathbf{e}}_y$ is along the chord to the arc forming the curved surface and $\hat{\mathbf{e}}_x$ is radially outward from the engine centerline. The transformational relationships between the two local coordinate systems are as follows:

$$\hat{\mathbf{e}}_t = \cos \Omega t \hat{\mathbf{i}} - \sin \Omega t \hat{\mathbf{k}} \quad (24)$$

$$\hat{\mathbf{e}}_a = \hat{\mathbf{j}} \quad (25)$$

$$\hat{\mathbf{e}}_r = \sin \Omega t \hat{\mathbf{i}} + \cos \Omega t \hat{\mathbf{k}} \quad (26)$$

$$\text{Thus, } \dot{\hat{\mathbf{e}}}_t = -\Omega \hat{\mathbf{e}}_r, \quad \dot{\hat{\mathbf{e}}}_a = 0 \quad \text{and} \quad \dot{\hat{\mathbf{e}}}_r = \Omega \hat{\mathbf{e}}_t. \quad (27)$$

The corresponding transformational equations in the matrix form between the two coordinate systems $(\hat{\mathbf{e}}_t, \hat{\mathbf{e}}_a, \hat{\mathbf{e}}_r)$ and $(\hat{\mathbf{e}}_x, \hat{\mathbf{e}}_y, \hat{\mathbf{e}}_z)$ are written as follows,

$$\begin{bmatrix} \hat{\mathbf{e}}_t \\ \hat{\mathbf{e}}_a \\ \hat{\mathbf{e}}_r \end{bmatrix} = \begin{bmatrix} 0 & -\sin(\phi_0 + \phi's + \theta) & -\cos(\phi_0 + \phi's + \theta) \\ 0 & \cos(\phi_0 + \phi's + \theta) & -\sin(\phi_0 + \phi's + \theta) \\ 1 & 0 & 0 \end{bmatrix} \begin{bmatrix} \hat{\mathbf{e}}_x \\ \hat{\mathbf{e}}_y \\ \hat{\mathbf{e}}_z \end{bmatrix} \quad (28)$$

The time derivatives of the respective unit vectors $(\hat{\mathbf{e}}_x, \hat{\mathbf{e}}_y, \hat{\mathbf{e}}_z)$ can be expressed as,

$$\dot{\hat{\mathbf{e}}}_x = -\Omega [\sin(\phi_0 + \phi's + \theta)\hat{\mathbf{e}}_y + \cos(\phi_0 + \phi's + \theta)\hat{\mathbf{e}}_z] \quad (29)$$

$$\dot{\hat{\mathbf{e}}}_y = [\phi's + \dot{\theta}]\hat{\mathbf{e}}_z + \Omega \sin(\phi_0 + \phi's + \theta)\hat{\mathbf{e}}_x \quad (30)$$

$$\dot{\hat{\mathbf{e}}}_z = -(\phi's + \dot{\theta})\hat{\mathbf{e}}_y + \Omega \cos(\phi_0 + \phi's + \theta)\hat{\mathbf{e}}_x \quad (31)$$

The corresponding absolute velocity vector $\dot{\vec{\mathbf{r}}}(s, \theta)$ of a point (in the global frame of reference) on the blade with (s, c) representing the time-dependent coordinate location of the bird-slice mass is derived as,

$$\begin{aligned} \dot{\mathbf{r}}(s, \theta) = & \begin{bmatrix} \dot{s} + \Omega r \cos \theta \cos(\phi + \theta) \\ -\Omega r \cos(\phi + \theta) - \Omega r \sin \theta \sin(\phi + \theta) \end{bmatrix} \hat{\mathbf{e}}_x \\ & - \begin{bmatrix} r' \dot{s} \sin \theta + r \cos \theta \dot{\theta} + (\phi' \dot{s} + \dot{\theta}) r (\cos \theta - 1) \\ + \Omega (R - L + s) \sin(\phi + \theta) \end{bmatrix} \hat{\mathbf{e}}_y \quad (32) \\ & + \begin{bmatrix} r' \dot{s} (\cos \theta - 1) - r \sin \theta \dot{\theta} \\ -(\phi' \dot{s} + \dot{\theta}) r \sin \theta - \Omega (R - L + s) \cos(\phi + \theta) \end{bmatrix} \hat{\mathbf{e}}_z \end{aligned}$$

Using the components of the absolute velocity vector of the bird-slice $\vec{\mathbf{V}}_a$ shown in Eq. (17), its relative velocity vector with respect to an observer sitting at the rotating blade is given by,

$$\vec{\mathbf{V}}_{\text{Relative}} = \vec{\mathbf{V}}_a - \dot{\mathbf{r}}(s, \theta) \quad (33)$$

i.e.

$$\begin{aligned} \vec{\mathbf{V}}_{\text{Relative}} &= V_x \hat{\mathbf{e}}_x + V_y \hat{\mathbf{e}}_y + V_z \hat{\mathbf{e}}_z \\ &= \begin{bmatrix} -\dot{s} - \Omega r \cos \theta \cos(\phi + \theta) \\ + \Omega r \cos(\phi + \theta) + \Omega r \sin \theta \sin(\phi + \theta) \end{bmatrix} \hat{\mathbf{e}}_x \\ &+ \begin{bmatrix} -V_a \cos \phi + \Omega (R - L + s) \sin(\phi + \theta) \\ + (r' \sin \theta - \phi' r (1 - \cos \theta)) \dot{s} + (2 \cos \theta - 1) r \dot{\theta} \end{bmatrix} \hat{\mathbf{e}}_y \quad (33) \\ &+ \begin{bmatrix} V_a \sin \phi + \Omega (R - L + s) \cos(\phi + \theta) \\ + (\phi' r \sin \theta + r' (1 - \cos \theta)) \dot{s} + 2r \sin \theta \dot{\theta} \end{bmatrix} \hat{\mathbf{e}}_z \end{aligned}$$

In the local blade curvilinear coordinates 'Normal-Tangential-Radial' ($\hat{\mathbf{e}}_n, \hat{\mathbf{e}}_\theta, \hat{\mathbf{e}}_r$) system the above equation Eq. (33) enables us to express the components of the relative velocity of the bird-slice mass in the directions normal, tangent and radial to the blade curved surface as,

$$V_n = -V_y \sin \theta + V_z \cos \theta \quad (34)$$

$$V_\theta = -V_y \cos \theta - V_z \sin \theta \quad (35)$$

$$V_r = V_x \quad (36)$$

Here, the normal component of the relative velocity vector V_n in Eq. (34) becomes the V_{impact} per Eq. (9). Thus, according to Eq. (10), the dynamic contact-impact load $F_{\text{slicing}}(t)$ during the slicing action with $B_a(t)$ being the instantaneous bird-foot-print-area, is computed as,

$$F_{\text{slicing}}(t) = B_a(t) \left[\frac{1}{2} \rho_B (V_n)^2 \right] \quad (37)$$

Also, the tangential component of the relative velocity vector V_θ in Eq. (35) causes the bird-slice mass to slide across the chord and is active for a time-duration called t_{travel} according to Eq. (13). After some lengthy algebraic manipulation, the corresponding relative acceleration vector $\ddot{\mathbf{r}}(s, \theta)$ of the bird-slice mass on the blade curvilinear surface is obtained as,

$$\ddot{\mathbf{r}}(s, \theta) = A_x \hat{\mathbf{e}}_x + A_y \hat{\mathbf{e}}_y + A_z \hat{\mathbf{e}}_z \quad (38)$$

where,

$$\begin{aligned} A_x &= \ddot{s} - \Omega^2 (R - L + s) \\ &- 2\Omega \dot{\theta} (r_0 + r's) \sin(\phi_0 + \phi's + 2\theta) \\ &+ 2\Omega (\phi' \dot{s} + \dot{\theta}) (r_0 + r's) \sin(\phi_0 + \phi's + \theta) \\ &- 2\Omega (\phi' \dot{s} + \dot{\theta}) (r_0 + r's) \sin(\phi_0 + \phi's + 2\theta) \\ &- 2\Omega r' \dot{s} \cos(\phi_0 + \phi's + \theta) \\ &+ 2\Omega r' \dot{s} \cos(\phi_0 + \phi's + 2\theta) \end{aligned} \quad (39)$$

$$\begin{aligned} A_y &= \ddot{s} [r' \sin \theta + (r_0 + r's) (\cos \theta - 1) \phi'] \\ &+ \ddot{\theta} [2 \cos \theta - 1] (r_0 + r's) \\ &+ 2\phi' r' (\dot{s})^2 (\cos \theta - 1) \\ &- (\phi' \dot{s})^2 (r_0 + r's) \sin \theta + 4r' \dot{s} \dot{\theta} \cos \theta \\ &- 4(\dot{\theta})^2 (r_0 + r's) \sin \theta \end{aligned} \quad (40)$$

$$\begin{aligned} &- 4\phi' \dot{s} \dot{\theta} (r_0 + r's) \sin \theta \\ &+ 2\Omega \dot{s} \sin(\phi_0 + \phi's + \theta) - 2r' \dot{s} \dot{\theta} \\ &- \Omega^2 (r_0 + r's) \sin(\phi_0 + \phi's + \theta) \\ &[\cos(\phi_0 + \phi's + \theta) - \cos(\phi_0 + \phi's + 2\theta)] \end{aligned}$$

$$\begin{aligned} A_z &= \ddot{s} [r' (\cos \theta - 1) - \phi' (r_0 + r's) \sin \theta] \\ &- 2(r_0 + r's) \sin \theta \ddot{\theta} - 2\phi' r' (\dot{s})^2 \sin \theta \\ &- 4(r_0 + r's) \cos \theta (\dot{\theta})^2 - 4r' \dot{s} \dot{\theta} \sin \theta \\ &- 2\Omega \dot{s} \cos(\phi_0 + \phi's + \theta) \\ &- 4\phi' \dot{s} \dot{\theta} (r_0 + r's) \cos \theta \\ &+ (\phi' \dot{s} + \dot{\theta})^2 (r_0 + r's) \\ &- (r_0 + r's) (\phi' \dot{s})^2 \cos \theta \\ &- \Omega^2 (r_0 + r's) \cos(\phi_0 + \phi's + \theta) \\ &[\cos(\phi_0 + \phi's + 2\theta) - \cos(\phi_0 + \phi's + \theta)] \end{aligned} \quad (41)$$

Thus,

$$A_n = -A_y \sin \theta + A_z \cos \theta \quad (42)$$

$$A_\theta = -A_y \cos \theta - A_z \sin \theta \quad (43)$$

$$A_r = A_x \quad (44)$$

Since the bird-slice is free to move in the span and the chord directions on the curvilinear surface of the pre-twisted blade without any resistance, we set $A_r = 0$ and $A_\theta = 0$. Thus, we obtain a set of coupled second-order non-linear differential equations with two unknowns (s, θ) as a function of time ' t ', which determine the time-history of the bird-slice mass trajectory. Once the coupled equations have been solved for the time-dependent parameters (s, θ), they are used to determine the acceleration ' A_n ' of the bird-slice mass B_m in the direction normal to the concave pressure surface of the blade, which yields the time-history of Coriolis forces as,

$$F_{\text{travel}}(t) = B_m A_n \quad (45)$$

The coupled set of non-linear differential equations of motion with $A_r = 0$ and $A_\theta = 0$ are solved numerically by a sixth-order Runge-Kutta method [30]. The initial conditions for the time-marching-forward solution are obtained from the impact conditions described in the bird-strike problem. As shown in Fig. 2, suppose the bird-cylinder makes initial contact with the turbofan blade at the span location of s_i , then the initial conditions for the numerical solution of the contact-impact forces would be described as,

$$s(0) = s_i \quad (46)$$

$$\theta(0) = -\frac{\vartheta}{2} \quad (47)$$

$$\dot{\theta}(0) = \frac{V_\theta(s_i, -\vartheta/2)}{r} \quad (48)$$

$$\dot{s}(0) = \frac{\begin{bmatrix} V_n - V_a \sin(\phi + \theta) \\ -\Omega(R - L + s_i) \cos(\phi + 2\theta) - r \sin \theta \dot{\theta} \end{bmatrix}}{[\phi' r \sin \theta - r'(1 - \cos \theta)]} \quad (49)$$

In the numerical scheme, it is assumed that the radius of curvature, ' r ', of the pressure side of the blade changes linearly from the root of the airfoil towards the tip. Similarly blade pre-twist angle ϕ changes linearly as the blade twist angle changes from ϕ_0 being at the root to twist-angle of ϕ_L being at the tip. The time-histories of the bird loading $F_{\text{Bird-slice}}$

from the current analytical model are being produced here in a non-dimensional form for a typical turbofan airfoil blade with the following parameters:

Fan outer radius	$R = 150$ cm
Span length of the blade	$L = 100$ cm
Blade average aspect ratio (L/C)	$L/C = 2.0$
Blade average camber radius	$r = 150$ cm
Total twist in the blade	$(\phi_L - \phi_0) = -60.0^\circ$
Number of fan blades on the disk	$N_b = 20$
Rotational speed	RPM = 3000
Angular velocity	$\Omega = 314.159$ rad/s
Blade tip tangential velocity	$V_t = 471.885$ m/s
Blade material density	$\rho = 4.443$ g/cm ³
Bird material density	$\rho_B = 0.9$ g/cm ³
Young's modulus of the blade material	$E = 117$ GPa
Aircraft velocity	$V_a = 100$ m/s

The typical trajectory of the bird-slice on the concave surface of the above hypothetical blade for a 75% span-shot is shown in Fig. 5. The graphical result shows that for this blade the bird-slice can move up by as high as 85.7% in the span-wise direction. The slice is propelled upward for about 2/3 of the chord travel, and then starts moving downward until it exits through the trailing edge at 84% span-height which is 9% higher than the initial entry contact location. In the plot the bird-slice is exiting at 104% of the initial chord, because the data has been normalized with respect to chord-size at the initial span-height. In the current formulation of the blade, the chord-size is increasing at the rate of C' as one moves from the root of the airfoil towards the blade-tip. In other words, if it is a constant chord blade, then rate of chord change parameter $C' = 0$.

A set of dynamic loads on the fan blade have been generated for different size birds such as 1 kg, 2 kg, 3 kg, and 4 kg bird-strike scenarios (see Fig. 6). Here, Fig. 6a, 6b and 6c are showing the family of curves for different bird sizes, for the initial impact location of 25%, 50% and 75% span, respectively. In these plots, for presenting the analytically predicted dynamic load time-history for a given size bird-slice we define the non-dimensional time term called \bar{t} as,

$$\bar{t} = t \left[\frac{\Omega}{2\pi} \right] \quad (50)$$

The bird-loading time-history shown here for varying impact locations on the blade leading edge enables us to identify the critical span location, which would result into maximum damage or largest strain to the fan blade.

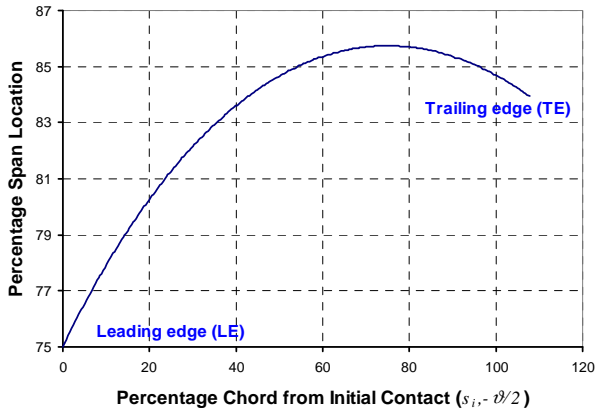


FIG. 5: Analytically computed bird-slice trajectory on the concave surface of an airfoil blade for a typical 75% span-shot.

The current analytical method of solving non-linear coupled partial differential equations provides a tremendous advantage in narrowing down the search for the critical location on the blade both for important design decisions about the leading edge thickness as well as any test planning. As an example, for this hypothetical fan configuration with $N_b = 20$ and $\bar{\Omega} = 0.058$ the critical span location has been determined as 43% span (see Fig. 7), in which case the peak dynamic contact-impact-slicing load for a typical 2 kg bird-strike can reach as high as 232 kN.

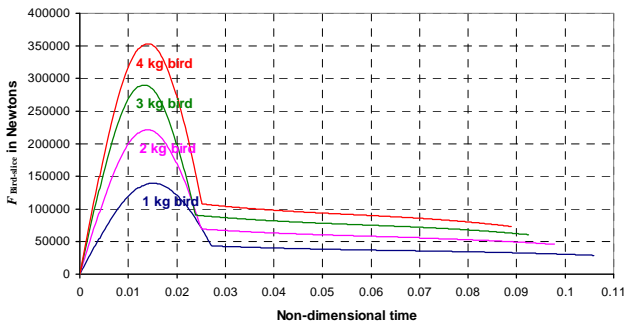


FIG. 6 (a) 25% span impact

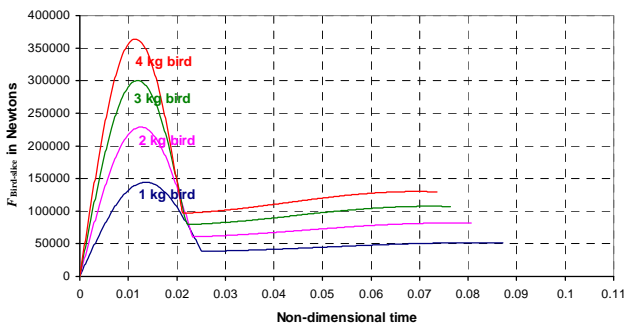


FIG. 6 (b) 50% span impact

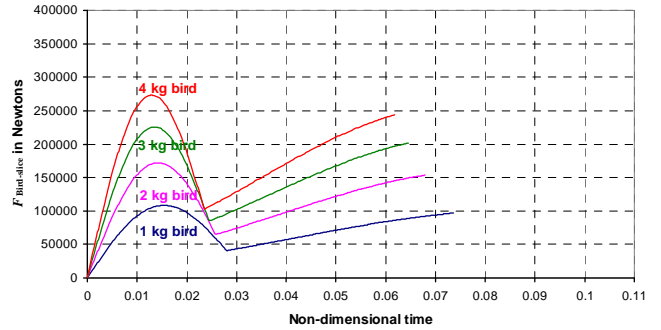


FIG. 6 (c) 75% span impact

FIG. 6: Time-history of contact-impact loads ($F(t)_{\text{Bird-slice}}$) on a typical fan blade ($L/C = 2$), by different size birds at the leading edge span locations (a) 25%, (b) 50%, (c) 75%.

These dynamic load curves can easily be scaled for evaluating some other fan blade design using dimensional scaling relationships. The peak dynamic load for a similar blade tip-velocity and a given bird-size will be,

(a) directly proportional to the square of the rotational angular velocity ratio, and,

(b) inversely proportional to the number of fan blades on the rotor .

For example, the dynamic load for a different rotational velocity of the fan, suppose Ω_0 , can be scaled as a square of the speed ratio given by,

$$F(t) = F(t)_{\text{Bird-slice}} \left(\frac{\Omega_0}{314.159} \right)^2 \quad (51)$$

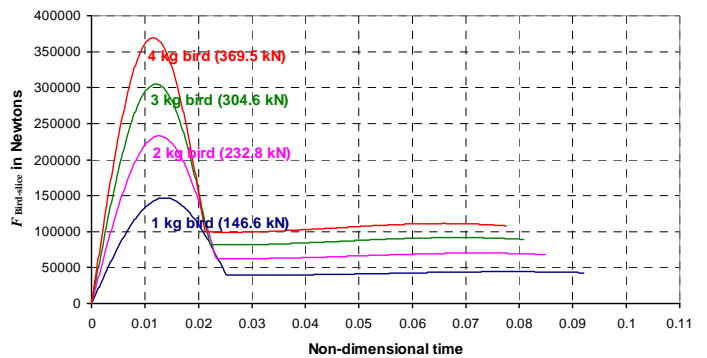


FIG. 7: Time-history of contact-impact loads ($F_{\text{Bird-slice}}$) on a typical fan blade ($L/C = 2$), by different size birds at the critical impact location of 43% of span.

The peak near-field span-wise strain at the blade leading edge develops at the end of bird-slicing event. For example in the critical bird-strike event shown in Fig. 7 for a 2

kg bird-strike scenario, the peak strain at the lead edge would develop at the instant $\bar{t} = 0.023$ whereas, the bird loading due to sliding on the pressure surface of the blade continues until $\bar{t} = 0.085$. After the travel time t_{travel} , bird-slice has exited beyond the blade-surface and the blade goes into free elastic oscillations in the centrifugal force-field as the post-impact dynamic response. Depending upon the blade design, sometimes the blade may exhibit higher strains at far-field locations as its post-impact dynamic response of free vibrations even after the primary bird-strike impact event is over.

4. VALIDATION OF BIRD AS A CYLINDER OF HYDRODYNAMIC MATERIAL

The analytical representation of bird model used in the current analysis in the form of a cylindrical-shape impactor is validated by a LS-DYNA simulation of a normal non-slicing impact on a flat panel representing a typical fan blade. Since, the objective of the test was focused on developing a proper material model to represent the dynamics of bird behavior, the controlled test was performed in such a way where the measured results should be free of any spurious loading complications caused by the slicing action of the blade leading edge. In the test set-up, a rectangular plate (Dimension: 43.18 cm long X 30.48 cm wide X 1.12 cm thick) plate was impacted in the middle by a gelatin bird weighing 161.7 gm moving at 92.66 m/sec (see Fig. 8). The gelatin-bird cylindrical impactor had a aspect ratio of $B_L / B_D = 2$ with outer diameter $B_D = 4.76$ cm. The dynamic strain-history due to simulated bird-strike were measured in two directions shown as SG_3 length-wise and SG_8 width-wise on the back-surface of the target plate.

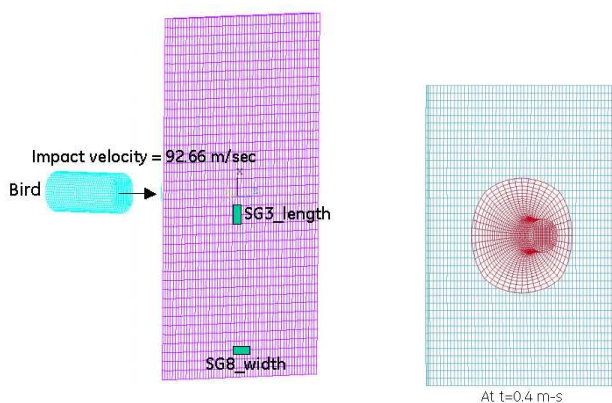


FIG. 8: (a) Rectangular composite panel with strain gages (SG3 and SG 8) being impacted by a bird-cylinder moving at 92.66 m/sec. (b) LS-DYNA results showing the deformation of a bird cylinder during the bird-strike after 0.4 m-seconds of initial contact

The controlled test condition simulating a typical bird-strike was represented in the analytical LS-DYNA modeling scheme. For this purpose, the bird material model was developed in the form of a hydrodynamic material with the equation of state representing the compressibility equation of a fluid mixture of made up of (10% air + 90% water). Fig. 8(b) shows the LS-DYNA produced typical analytical results at 0.4 m-seconds highlighting the spreading action of the bird material during the bird-strike.

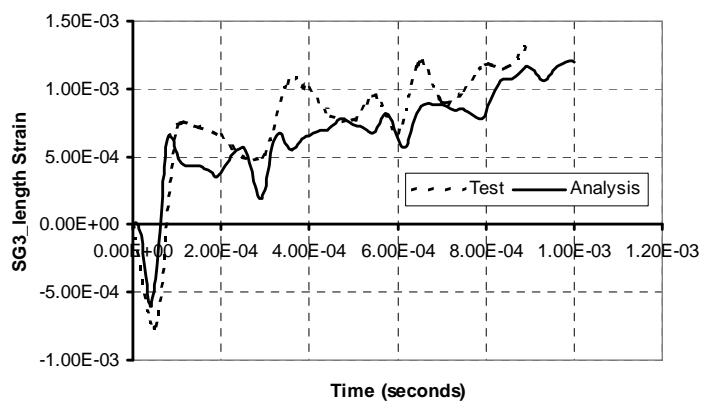


FIG. 9 : Comparison of Strain gage dynamic response from LS-DYNA vs. Test data (Lengthwise strain gage - SG3)

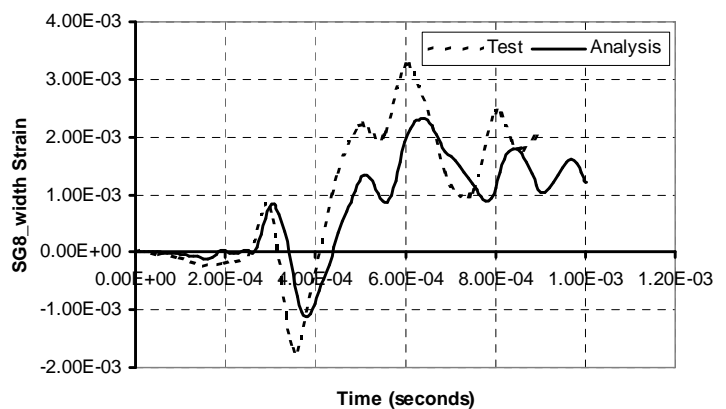


FIG. 10: Comparison of Strain gage dynamic response from LS-DYNA vs. Test data (Widthwise strain gage - SG8)

Figs. 9 and 10 show the comparison of measured versus analytically predicted strain results for two typical gages using the hydrodynamic material model (10% air + 90% water) to represent the loading characteristics of the bird. Numerically computed strain gage response results based upon the fluid bird model compare very well with the measured data from the

actual test both in magnitude as well as in frequency contents of the dynamic response. Overall, the comparison of the predicted vs. measured surface strain results show that the bird model developed in the current paper produces reasonably good correlation with the test data and can be used reliably for analyzing many different types of complex bird-strike loading scenarios including slicing impact.

4.1. Comparison of bird-strike loads from the current analytical model vs. LS-DYNA results

We have also established the accuracy of current analytical model in predicting the peak magnitude of transient dynamic loads by running a highly detailed LS-DYNA simulation of the hypothetical blade described in section-3. The LS-DYNA model developed for this purpose is shown in Fig. 11. In this simulation a 2 kg bird hits a 3-bladed sector of 20-bladed turbofan rotor at 43% span.

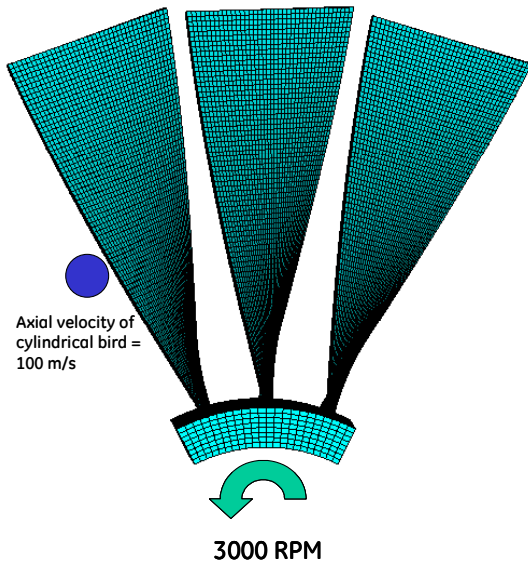


FIG. 11: LS-DYNA simulation of a 2 kg bird-strike on a 3-bladed sector of a typical turbofan rotor

In this analysis, the bird is modeled as a cylinder with $B_L / B_D = 2$ and approaching the fan rotor blades at 100 m/sec.. The bird cylinder gets sliced as its is described earlier in the section-2 of this paper. In a multiple blade slicing event the first two blades get full-size slice and the last blade gets impacted only by remaining partial slice. The other relevant bird and slicing parameters for this impact condition are summarized as follows.

Bird cylinder diameter	$B_D = 11.23$ cm
Bird cylinder length	$B_L = 22.46$ cm
Axial length of bird 'Ideal slice'	$B_s = 10.00$ cm

Bird slice mass	$B_m = 891.4$ g
Tangential velocity	$V_t = 292.17$ m/s
Bird slicing time	$t_{\text{slicing}} = 0.384 \times 10^{-3}$ s
Number of blades with full-size slice	$N_B = 2$

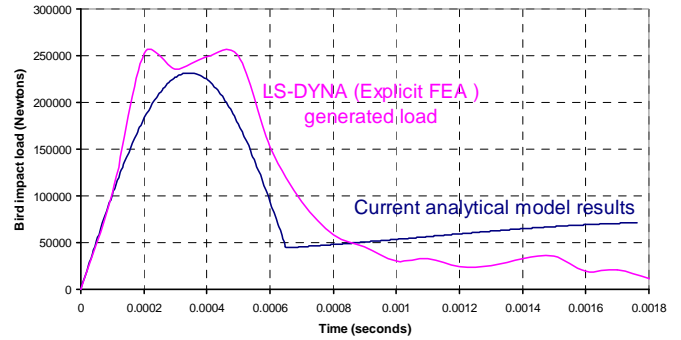


FIG. 12: Time-history of the bird-slice load in the tangential direction of the fan-rotor on a 20 bladed rotor due to 2 kg bird at 100 m/s.

Fig. 12 shows the comparison of the load time-history from the current physics-based partial differential equation versus LS-DYNA generated results. The force-history plot clearly shows that for this hypothetical fan blade the loading time $t_{\text{loading}} = 1.8$ milliseconds out of which first 0.7 milliseconds shows impulsive characteristics, which is acting at the blade leading edge in the vicinity of the initial contact location. The results indicate that for a typical fan blade in a running condition, the present physics-based solution captures the qualitative time-domain characteristics of the bird-strike impact force-history reasonably well. This is especially true during the slicing phase, where it has been shown to capture the individual peak dynamic load to within 9% as compared to the LS-DYNA simulated peak load. The impact load shown in Fig. 12 produces impulsive torque on the fan-shaft, which in a multiple blades bird-strike scenario may be computed by superimposing these individual load-histories data with initial offset on the time-scale to take into account of the blade separation in the circumferential direction of the rotor.

5. TRANSIENT RESPONSE OF ROTATING AIRFOIL BLADES DUE TO BIRD-STRIKE LOADS

The transient dynamic response of the structure due to bird-strike loads is the main interest during the mechanical design of the airfoil blades. The out-of-plane deflection and the resulting strains in the blade can be calculated analytically from a physics-based model, which needs to be validated by experimental measurements as well [32]. In this section we will briefly describe as to how the contact-impact loads called

$F_{\text{Bird-slice}}$ can be used as an external forcing function for determining the time-domain dynamic response of the deformable turbofan blade during bird-strike. For this discussion, we will use standard Timoshenko's [33] plate theory notations. Based upon the classical Kirchoff-von Karman's plate bending formulation [34], the general equation for the flexural motion $w(x, y, t)$ in the transverse direction (z -axis) along with the rotary and warping inertias of a pre-twisted rectangular plate with the in-plane distributed membrane forces N_x and N_y respectively, is written as:

$$\begin{aligned}
& D \left[\frac{\partial^4 w}{\partial x^4} + 2 \frac{\partial^4 w}{\partial x^2 \partial y^2} + \frac{\partial^4 w}{\partial y^4} \right] \\
& + D(\phi')^2 \left[3 \frac{\partial^2 w}{\partial x^2} + \frac{\partial^2 w}{\partial y^2} \right] \\
& - D(\phi')^4 \left[x^2 \frac{\partial^2 w}{\partial x^2} + \frac{(1-\nu)}{2} x^2 \frac{\partial^2 w}{\partial y^2} + 2x \frac{\partial w}{\partial x} \right] \\
& - \frac{\partial}{\partial x} \left[N_x \frac{\partial w}{\partial x} \right] - \frac{\partial}{\partial y} \left[N_y \frac{\partial w}{\partial y} \right] \\
& - \rho h \Omega^2 \cos^2 \phi w + 2 \rho h \Omega x \frac{\partial \dot{w}}{\partial x} \\
& = -\rho h \frac{\partial^2 w}{\partial t^2} + \rho \frac{h^3}{12} \frac{\partial^2}{\partial t^2} \left(\frac{\partial^2 w}{\partial x^2} + \frac{\partial^2 w}{\partial y^2} \right) \\
& - \rho h (\phi' x)^2 \left[\frac{\partial^2 w}{\partial t^2} - \nu \left(\frac{C y}{L} \right)^2 \frac{\partial^4 w}{\partial y^2 \partial t^2} \right] + q(x, y, t)
\end{aligned} \tag{52}$$

Here, the in-plane distributed membrane forces N_x and N_y are caused by the centrifugal forces. The Coriolis force $2\rho h \Omega x \frac{\partial \dot{w}}{\partial x}$ in the blade is generated due to the velocity component caused by its movement along the engine axis. Here it should be noted that in the rotating condition of a pre-twisted airfoil, while the longitudinal component (span-wise) of the centrifugal forces $(\sigma_{cf})_x$ result into stiffening of the blade, its chord-wise component $(\sigma_{cf})_y$ tries to soften the blade by untwisting the airfoil cross-section. We obtain the relationships for $(\sigma_{cf})_x$ and $(\sigma_{cf})_y$ due to the angular velocity Ω in a rectangular plate with a pre-twist of $\phi(x)$ at any typical point located at (x, y) as,

$$\left. \begin{aligned}
\frac{N_x}{h} = (\sigma_{cf})_x &= \frac{\rho \Omega^2}{2} \left[L(2R-L) - 2(R-L)x - x^2 \right] \\
\frac{N_y}{h} = (\sigma_{cf})_y &= -\frac{\rho C^2 \Omega^2 \sin^2(\phi_0 + \phi' x)}{8}
\end{aligned} \right\} \tag{53}$$

In Eq. (16) the right-hand-side external load vector term $q(x, y, t)$ being expressed as pressure applied per unit area is obtained by converting the dynamic contact-impact load $F_{\text{Bird-slice}}$ due to bird-strike at a location (s, c) of the plate pressure surface in shell coordinates using Dirac's delta impulse functions $\delta(x-s)$ and $\delta(y-c)$ as,

$$q(x, y, t) = [-B_m \ddot{w} + F_{\text{Bird-slice}}] \delta(x-s) \delta(y-c) \tag{54}$$

In the above equation, the time-dependent coordinate location (s, c) of the bird-slice is determined by solving the trajectory equation as shown in Fig. 5. Here, it should be recalled that by definition the dimensions of the Dirac's delta function is always L^{-1} . In the present paper our focus is on determining the time-dependent forcing function $F(t)_{\text{Bird-slice}}$ for different size birds as bird comes in contact with a rotating engine.

6. SUMMARY AND CONCLUSIONS

It is a common practice to simulate the airfoil blades used in rotating machinery by a pre-twisted cantilever plates to its exact shape and profile using finite-element representation. In normal operation, these blades may be subjected to many different types of impact loading scenarios known as FOD (Foreign Object Damage). In order to evaluate the dynamic response of these blades under FOD-related impact conditions, one needs a precise description of the time-dependent history of the forcing function. These contact-impact forcing functions are highly non-linear in nature [35] and have been difficult to determine by any analytical means especially in soft-body impact situations like a bird-strike on a fan blade.

The mathematical formulation presented here enables us to determine the transient contact-impact load time-history $F_{\text{Bird-slice}}$ in a physics based analytical model. In this paper, we determine the size, shape and the mass of the birds-slice as a function of the bird-weight and the relative velocity of the aircraft and the running speed of the turbofan rotor. The approach of bird material modeling established in this paper has been validated by a controlled test and by replicating the results using the similar hydrodynamic material model in LS-DYNA. The slicing load time-history equation is developed as a function of the normal component of the relative impact velocity vector and treating the bird like a hydrodynamic material in the shape of cylinder with the length-to-diameter

ratio equal to 2. Using the initial contact velocity of the bird-cylinder we determine the load time-history and the duration of slicing action by the leading edge of the blade. In the present analysis the bird slice has been simulated as a projectile which gets accelerated as it moves upward on the concave surface of the blade. The full derivation of the non-linear dynamical equations have been presented, and are solved in the time-domain by using a sixth-order Runge-Kutta method. The normal component of the bird slice acceleration is used to determine the dynamic load time-history on the pressure surface of the airfoil blade. The load time-history is presented in a non-dimensional form for various bird-sizes for 3 different span locations. The accuracy of the predicted peak magnitude of the dynamic load may be further improved by incorporating a more complex function to represent the bird foot-print area, $B_a(t)$, of Eq. 10. In the current solution a relatively simple sinusoidal distribution is assumed.

This modeling also provides the critical impact location, which is an important requirement as established for any ingestion test acceptable to regulatory agencies like the FAA [1]. The critical location for the bird-strike test is different for each blade design and the FAA requires that it be identified accurately by the engine manufacturer before the bird-ingestion test-plan gets approved. This paper also briefly discusses the flexural stress-wave differential equation approach to determine the transient response of the airfoil blade in terms of dynamic stresses being developed during the bird-strike. Furthermore, it is conceivable that the bird-strike loading determined in this fashion can also be used to determine the dynamic response of turbofan blades and even full engines [36].

ACKNOWLEDGMENTS

The authors would like to thank their manager Mr. Darin DiTommaso for his support and encouragement about getting this work published.

7. REFERENCES

- [1] Code of Federal Regulations: Aeronautics and Space, 1990, Art. 33.76, Vol. 14, Office of the Federal Register, National Archives and Record Administration, Washington, DC.
- [2] S. Georgiadis, A.J. Gunnion, R.S. Thomson, and B.K. Cartwright, 2008, "Bird-strike simulation for certification of the Boeing 787 composite moveable trailing edge", *Composite Structures*, **86** (1-3), pp. 258-268.
- [3] E. Niering, 1990, "Simulation of Bird Strikes on Turbine Engines", *ASME J. Eng. for Gas Turbine and Power*, **112**, pp. 573-578.
- [4] N.F. Martin, Jr., 1990, "Nonlinear Finite-Element Analysis to predict Fan Blade Damage Soft Body Impact", *J. of Propulsion*, **86**, pp. 445-450.
- [5] R. Jain, and K. Ramchandra, 2003, "Bird Impact Analysis of Pre-stressed Fan Blades using Explicit Finite Element Code", IGTC 2003 Tokyo TS-009, *Proc. Of the Int. Gas Turbine Congress, Tokyo*, November 2-7, 2003, 7 pages.
- [6] M. A. McCarthy, J.R. Xiao, C.T. McCarthy, A. Kamoulakos, J. Ramos, J.P. Gallaard and V. Melito, 2004, "Modeling of Bird-strike on an Aircraft Wing Leading edge made from Fiber Metal Laminates", *Appl. Composite Materials*, **11** (5), pp. 317-340.
- [7] V.K. Goyal, C.A. Huertas, J. R. Borrero, and T.R. Leutwiler, 2006, "Robust Bird-strike Modeling Based on ALE Formulation using LS-DYNA", *47th AIAA/ASME/ASCE/AHS/ASC Structures, Structural Dynamics and Materials Conference, Newport, Rhode Island*, 4 May 2006, Paper No. AIAA 2006-1759, 18 pages.
- [8] L.E. Schwer, and R.G. Whirley, 1999, "Impact of a 3D Woven Textile Composite Thin Panel: Damage and Failure Modeling", *Mechanics of Composite Materials and Structures*, **6** (1), pp. 9-30.
- [9] B. Langrand, A-S Bayart, Y. Chauveau, E. Deletombe, 2002, "Assessment of multi-physics FE methods for bird strike modelling - Application to a metallic riveted airframe", *Int. J. Crashworthiness*, **7** (4), pp. 415 - 428.
- [10] A.F. Johnson and M. Holzapfel, 2006, "Numerical prediction of damage in composite structures from soft body impacts", *J. Materials Science*, **41** (20), pp. 6622-6630.
- [11] I. Smojver, and D. Ivančević, 2010, "Numerical simulation of bird strike damage prediction in airplane flap structure", *Composite Structures*, **92** (9), pp. 2016-2026.
- [12] M. Guida, F. Marulo, T. Polito, M. Meo, M. Riccio, 2009, "Design and testing of a fiber-metal-laminate bird-strike-resistant leading edge", *J. of Aircraft*, **46** (6), pp. 2121-2129.
- [13] S. K. Sinha, and N. Jain, 2007, "Soft-body impact on jet engine components made-up of composites", *International SAMPE Technical Conference*, Cincinnati, OH.
- [14] T. Kermanidis, G. Labeas, M. Sunaric, A.F. Johnson, M. Holzapfel, 2006, "Bird strike simulation on a novel composite leading edge design", *Int. J. Crashworthiness*, **11** (3), pp. 189-201.

- [15] M.A. McCarthy, J.R. Xiao, N. Petrinic, A. Kamoulakos, V. Melito, 2005, "Modelling bird impacts on an aircraft wing - Part I: Material modelling of the fibre metal laminate leading edge material with continuum damage mechanics", *Int. J. Crashworthiness*, **10** (1), pp. 41-49.
- [16] W. Xinjun, F. Zhenzhou, W. Fusheng and Y. Zhufeng, 2007, "Dynamic response analysis of Bird Strike on Aircraft windshield based on Damage-modified nonlinear viscoelastic constitutive relation", *Chinese J. Aeronautics*, **20**, pp. 511-517.
- [17] M. Guida, F. Marulo, M. Meo and M. Riccio, 2008, "Analysis of Bird impact on a Composite Tailplane Leading Edge", *Appl. Composite Materials*, **15**, pp. 241-257.
- [18] A.G. Hanssen, Y. Girard, L. Olovsson, T. Berstad, M. Langseth, 2006, "A numerical model for bird strike of aluminium foam-based sandwich panels ", *Int. J. Impact Eng.*, **32**, pp. 1127-1144.
- [19] A. Airolidi, B. Cacchione, 2006, " Modelling of impact forces and pressures in Lagrangian bird strike analyses", *Int. J. Impact Eng.*, **32** , pp. 1651-1677.
- [20] H. C. Teichman, and R. N. Tadros, 1991, "Analytical and Experimental Simulation of Fan Blade Behavior and Damage under Bird Impact", *ASME J. Eng. for Gas Turbine and Power*, **113**, pp. 582 - 594.
- [21] R.H. Mao, S.A. Meguid, T.Y. Ng, 2008, " Transient three dimensional finite element analysis of a bird striking a fan blade", *Int. J. Mechanics and Materials in Design*, **4** (1), pp. 79-96.
- [22] M. A. Lavoie, A. Gakwaya , M. Nejad Ensam, and D.G. Zimcik, 2007, "Review of existing numerical methods and validation procedure available for bird strike modeling", *ICCES*, **2** (4), pp. 111-118.
- [23] Y.A. Khulief , 2010, "Numerical Modeling of Impulsive events in Mechanical Systems", *Int. J. Modelling and Simulation*, **30** (1), pp. 80-86.
- [24] K.N. Shivkumar, W. Elber and W. Illg, 1985, "Prediction of Impact Force and duration due to Low-velocity Impact on Circular Composite Laminates", *ASME J. Appl. Mech.*, **52** (3), pp. 674-680.
- [25] S. K. Sinha and M. M. Zentner, 1986, "Dynamic Bending Stresses in Thin Elastic Plates due to Impact by Spherical Projectile", 10th U.S. National Congress of Applied Mechanics, University of Texas at Austin, TX .
- [26] J.F. Doyle, 1987, "Experimentally determining the contact force during the transverse impact of an orthotropic plate", *J. Sound and Vibration*, **118** (3), pp. 441-448.
- [27] K. Hemmi, M. Nishikawa, and N. Takeda, 2008, "Prediction of the foreign-object impact force on the composite fan blade" , *Design, Manufacturing and Applications of Composites: Proceedings of the 7th Joint Canada-Japan Workshop on Composites*, pp. 101-108.
- [28] J.S. Wilbeck and J.L.Rand, 1981, "The development of a substitute Bird model", *ASME J. Eng. for Power*, **103**, pp. 725-730.
- [29] H. Kim and K. T. Kedward, 2000, "Modeling Hail Ice Impacts and Predicting Impact Damage Initiation in Composite Structures", *AIAA Journal*, **38** (7), pp. 1278-1288.
- [30] E. Fehlberg, 1964, "New high order Runge-Kutta formulas with stepsize control for systems of first- and second order differential equations", *Zeitschrift für Angewandte Mathematik und Mechanik (ZAMM)*, **44**, pp. 17-29.
- [31] R. Olsson, 2003, "Closed form prediction of peak load and delamination onset under small mass impact", *Composite Structures*, **59**, pp. 341-349.
- [32] W. Van Paepegema,, A. Shulev, A. Moentjens, J. Harizanova, J. Degrieck, V. Sainov, 2008, "Use of projection moiré for measuring the instantaneous out-of-plane deflections of composite plates subject to bird strike", *Optics and Lasers in Eng.* , **46** , pp. 527 - 534.
- [33] S. Timoshenko, and S. Woinowsky-Krieger, 1959, 'Theory of Plates and Shells ', 2nd edition, McGraw-Hill Book Co., New York, pp. 378-380.
- [34] S.K. Sinha and K.E. Turner, 2011, "Natural Frequencies of a Pre-twisted blade in a Centrifugal Force Field", *J. Sound and Vibration* , doi: 10.1016/j.jsv.2010.12.017.
- [35] S. K. Sinha, 2007, "Combined Torsional-Bending-Axial Dynamics of a Twisted Rotating Cantilever Timoshenko Beam with Contact-Impact Loads at the Free End", *ASME J. Appl. Mech.*, **74**, pp. 505-522.
- [36] S.K. Sinha, and S. Dorbala, 2009, "Dynamic Loads in the Fan Containment Structure of a Turbofan Engine ", *ASCE J. Aerospace Eng.*, **22** (3), pp. 260-269.